JOURNAL OF CATALYSIS 157, 559–568 (1995)

Reaction of Coadsorbed Nitric Oxide and Nitrogen Atoms on Rh(111)

David N. Belton,*,[1] Craig L. DiMaggio,* Steven J. Schmieg,* and K. Y. Simon Ng†

*Physical Chemistry Department, General Motors Research and Development Center, Building 1-6, 30500 Mound Road, Box 9055, Warren, Michigan 48090-9055; and †Department of Chemical Engineering, Wayne State University, Detroit, Michigan 48202

Received September 23, 1994; revised June 8, 1995; accepted July 12, 1995

We have studied the reaction of nitrogen atoms (N) with nitric oxide molecules (NO) coadsorbed on a Rh(111) catalyst in order to isolate the reaction of these two species as an elementary step (e.g., in the NO + CO reaction mechanism) and determine the products of that reaction. Electron beam dissociation of adsorbed NO was used to cleanly prepare N atom coverages between 0.05 and 0.5 monolayers. By using isotopically labeled NO and N reactants, we determined that NO and N react, under our conditions, to form only N_2O. In contrast to previous reports, we see no evidence that suggests that NO and N can react to form N_2 as a product. In complementary experiments, we have completed computer modeling of an NO temperature-programmed desorption experiment. These simulations show that NO dissociation rates in the high NO coverage limit are as much as 500 times slower than previously reported dissociation in the low coverage limit. © 1995 Academic Press, Inc.

1. INTRODUCTION

Beginning in 1994, government regulations mandate that vehicle emissions for both hydrocarbons (HC) and nitrogen oxides (NO_x) must fall substantially from current levels. Currently, roughly half of all regulated CO and HC emissions during the Federal Test Procedure (FTP) test occur early in the test before the catalytic coverter reaches a temperature sufficiently high to become active (light-off). However, NO_x emissions are spread more evenly over the entire test, owing to the fact that NO_x kinetics are much more problematic than those for CO and HC. One of the keys to meeting the more stringent future NO_x emissions standards will be to gain a better understanding of why NO_x emissions occur and how to reduce those emissions. In order to better understand the mechanism for the reduction of NO by CO we have a continuing program to define and understand the reaction kinetics responsible for conversion of pollutants (in this case NO) into unregulated products (N_2). For this work we use kinetic measurements over single crystal catalysts, primarily because they offer the best systems for detailed understanding of reaction kinetics and mechanisms. This statement is true primarily because single crystals are amenable to measurements of the rates of individual or elementary steps in the mechanism. Without measurements of the rates of at least some of the elementary steps it is virtually impossible to verify/eliminate a given reaction mechanism.

The experiments we report here make a significant contribution to the understanding of NO reduction by CO. There have been a number of papers on the NO–CO reaction over supported Rh(1–7) and Pt–Rh (8–10) catalysts in addition to several papers on Rh (11–18) and Pt–Rh (19–21) single crystal catalysts. In a previous paper we reported the reaction rates and product distributions for the NO–CO reaction over Rh(111) at moderate pressures (1–100 Torr) (22). More recently we have compared those Rh(111) kinetics to those of a Rh(110) catalyst (23). For both Rh(111) and Rh(110), N_2 and N_2O were observed as reaction products of the NO–CO reaction. When reacted over Rh(111) the selectivity for N_2O is remarkably insensitive to reaction conditions; however, the more open Rh(110) surface showed a strong tendency to switch over from making large amounts of N_2O to making predominately N_2 as the reaction conditions were charged (23). Although it is an important product, our knowledge of N_2O formation is meager.

Several different reaction mechanisms for the NO–CO (1, 3–5, 7, 11, 17, 22) reaction have been put forth over the years. For completeness and ease of subsequent discussion we simply list all of the reaction steps that have been proposed as part of NO–CO mechanisms. They are:

$$CO_g + S \Leftrightarrow CO_a \quad [1]$$

$$NO_g + S \Leftrightarrow NO_a \quad [2]$$

$$NO_a + S \Rightarrow N_a + O_a \quad [3]$$

$$CO_a + O_a \Rightarrow CO_{2g} + 2S \quad [4]$$

$$NO_a + N_a \Rightarrow N_2O_a + S \quad [5]$$

$$NO_a + N_a \Rightarrow N_{2g} + O_a + S \quad [6]$$

[1] To whom correspondence should be addressed. Fax: (810) 986-8697. E-mail: dbelton@cmsa.gmr.com.

0021-9517/95 $12.00

$$N_2O_a \Rightarrow N_2O_g + S \quad [7]$$

$$N_2O_a \Rightarrow N_{2g} + O_a \quad [8]$$

$$N_a + N_a \Rightarrow N_{2g} + 2S. \quad [9]$$

In this paper, we deal exclusively with steps [2], [3], [5], and [6] focusing on two issues. First, we wish to get better estimates of the rate for NO dissociation and the rate for desorption at high NO coverges that are most applicable to those pressure/temperature conditions found in automotive catalytic converters. Previously reported NO dissociation rates, step [3], were based on measurements made with relatively low, <0.1 monolayer (ML), NO coverages (19). In addition, previous rate parameters for NO desorption (11) were derived using Chan and Wienberg's (see Ref. 24) method, which uses the width and peak maximum of the desorption feature. This method may be subject to some error in a system such as NO desorption in which both desorption and dissociation are occurring simultaneously.

Second, we wanted to know if there was any experimental evidence for reaction [6], NO + N → N_{2g}. For Rh surfaces, this elementary step was initially proposed (12, 15, 25) or suggested (26) by several different groups based primarily on temperature-programmed desorption (TPD) data from adsorbed NO. When adsorbed NO is desorbed from Rh surfaces, either supported Rh (25, 27) or Rh single crystals (12, 28, 29), some gas phase N_2 is also produced in two distinctly separate peaks. At low initial NO coverages, no NO desorbs from the surface and N_2 is evolved in a single, second-order peak that is assigned to N atom recombination of dissociated NO. At higher initial NO coverages a second N_2 desorption feature is observed at exactly those NO coverages where NO desorption is first observed. In addition, the N_2 and NO desorption features occur at temperatures within 20 K of one another. Over some supported catalysts (25), N_2O is also observed in this temperature regime (25). The strong correlation between NO, N_2, and N_2O desorption was taken as evidence that N_2O and N_2 were formed via a common "N_2O-like" intermediate (N_2O*) (12, 15, 25). Following these early papers, it became common for the NO + N → N_{2g} + O reaction to appear in NO reduction mechanisms (1, 3–5, 7, 11, 17). When the concept of a common N_2O-like intermediate was applied to the NO–CO reaction, it was suggested that the selectivity is controlled by the relative rates of disproportionation to give N_2 and desorption to give N_2O (1, 7). A second NO–CO mechanism in the literature is one that was formulated to explain the activity over both single crystal Rh and supported Rh catalysts (11). This second mechanism differs from the first primarily in that it has N_2 formed by two different pathways: NO + N → N_{2g} at low temperatures and N + N → N_2 at high temperatures. The experiments reported in this paper were specifically designed to test the idea that N_2O and N_2 come from a common intermediate. Our results show conclusively that NO + N → N_2O* → N_{2g} does not occur during an NO TPD experiment and consequently there is no experimental evidence for this reaction step. We recommend that future NO reduction mechanisms omit this step unless it is required to explain the observed kinetic data or some experimental data are obtained in support of this process.

2. METHODS

2.1. Apparatus

The experiments were performed in a standard ion-pumped vacuum system similar to that described elsewhere (13). The system is equipped with a double-pass cylindrical mirror analyzer for Auger electron spectroscopy (AES), a four-grid LEED system, a high-resolution electron energy loss (HREELS) spectrometer, and an apertured quadrupole mass spectrometer (QMS) for temperature-programmed desorption. The Rh(111) surface was oriented to within ±1° of the desired crystallographic direction and polished with 1/4-μm diamond polish prior to mounting. The sample was mounted with Ta wires spot-welded on the back of the crystal to allow for resistive heating and liquid nitrogen cooling. The crystal was cleaned with cycles of sputtering at 875 K using 2.5-KeV Ar ions, followed by annealing to 1350 K until all AES detectable contaminants (except carbon) were removed and sharp LEED patterns were obtained. At this point the C was removed by slow cycling under a flux of O_2 between 800 and 1250 K. This procedure removed C from both the surface and the near-surface regions of the crystal. Subsurface C migrates to the surface at high temperatures, reacting with surface O atoms to make CO (14). All TPD spectra were taken with the crystal placed about 2 mm from the aperture of the QMS. The sample was heated at 10 K/s and nine masses were obtained simultaneously during the experiment.

2.2. N Atom Preparation

In order to obtain high N atom coverages, four thoriated iridium filaments were mounted in parallel on Ta posts to provide electrons to bombard preadsorbed NO on Rh(111). Typically, NO was admitted through a doser, raising the background pressure by 5×10^{-11} Torr. The Rh(111) crystal was held at 120 K and, when it was in front of the doser, a saturation NO coverage was achieved within 30 s. Next, the sample was placed about 5 mm from the electron source with a +100-V bias applied to the sample and the filament current adjusted so that 1.2 mA of current was passed to the Rh(111) crystal for 5 min. During bombardment the sample temperature increased from 120 to 150 K. When the sample was examined with AES after e^-

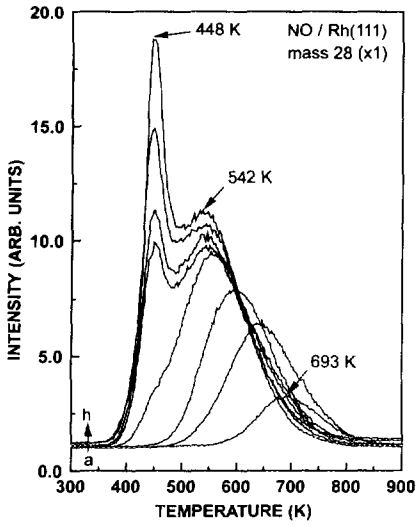

FIG. 1. N_2 desorption detected after adsorption of NO at 200 K. NO exposures, given in doser-seconds, for curves (a)–(h) are: 0.5, 1, 1.5, 2, 4, 5, 8, 15, respectively.

beam bombardment, we found that most of the oxygen had been removed from the surface. The high N/O ratio (≈8 N per O) indicates that significant NO dissociation occurs during bombardment and that the dissociation occurs via electron-stimulated desorption of oxygen. Next, the sample was heated to at least 415 K (higher temperatures if lower N coverages were desired) to remove any residual NO that might remain on the surface. Finally, we used absorbed CO to clean off (via CO_2 formation) the oxygen contamination that might still be present. The oxygen cleaning procedure was as follows: (i) about 3 L of CO was dosed at 120 K, (ii) the surface was heated to at least 415 K (higher if lower N coverages were desired), (iii) the surface was cooled to 120 K, and the process repeated. We estimate that under the worst conditions, residual oxygen coverages were approximately 0.05 ML (from AES and TPD) and residual CO coverages (CO desorbs at lower temperatures than does N) were about 0.1 ML.

In these experiments we used both ^{15}NO and ^{14}NO that were nominally of 98% purity. For both gases the major impurity was N_2 of the same isotopic label. Amounts of the other N isotope were below 1% and thus were not experimentally detectable in a TPD experiment.

2.3. *Modeling of NO TPD*

In Section 3.3 we discuss the results of some kinetic modeling of the NO TPD experiment (Figs. 1 and 2) that we carried out in order to learn more about the rates of NO desorption and dissociation. In order to model the NO TPD data presented in Figs. 1 and 2 we require (i) a mechanism, (ii) rate expressions for each step in the mechanism, (iii) rate constants for each step, and (iv) a set of conservation equations for the surface species. Based on our experimental observations (NO + N reaction does not form N_2 in a TPD experiment and no N_2O is formed over Rh(111)) we included the following elementary steps in our NO TPD model:

$$NO_a \Rightarrow NO_g + S_\nu^{atop} \quad [10]$$

$$NO_a + S_\nu^{atop} + 2S_\nu^{hollow} \Rightarrow N_a + O_a + 2S_\nu^{atop} \quad [11]$$

$$N_a + N_a \Rightarrow N_{2g} + 2S_\nu^{hollow} \quad [12]$$

$$O_a + O_a \Rightarrow O_{2g} + 2S_\nu^{hollow}. \quad [13]$$

Once we propose a mechanism, our next requirement is a rate expression for each step. For NO desorption we choose to use a straight first-order NO desorption rate of the form:

$$R_{des}^{NO} = \nu \exp\left(\frac{-E_a}{RT}\right) \Theta_{NO}.$$

For NO dissociation our expression is slightly more complicated than those previously proposed (11). It is:

$$R_{diss}^{NO} = \nu \exp\left(\frac{-(E_a + \alpha_{NO}\Theta_{NO})}{RT}\right) \Theta_{NO}\Theta_{\nu,hollow}^2\Theta_{\nu,atop}.$$

The most significant aspect to this rate expression is the requirement of two types of vacant sites, atop sites and

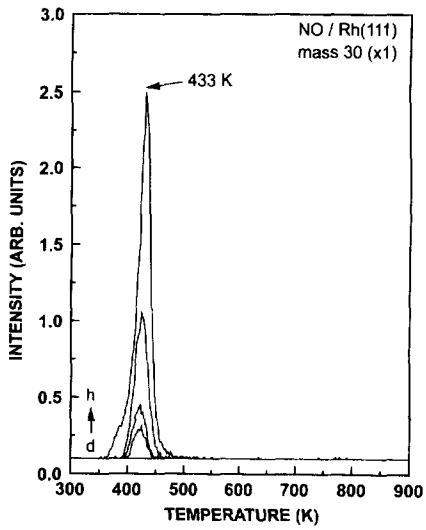

FIG. 2. NO desorption detected after adsorption of NO. Data were taken concurrently with the data of Fig. 1. For exposures below 2 doser-sec, no NO desorption was detected. Figure 2 uses the same designations as Fig. 1 and shows data for curves (d)–(h) for which the exposures were 2, 4, 5, 8, and 15 doser-sec, respectively.

hollow sites. We incorporate these two requirements because (i) it is known that the dissociation products, N and O, adsorb into the threefold hollow sites on the Rh(111) surface, and (ii) it has been observed that vacant atop sites are required in order for NO to dissociate on Rh(111) (12–14). Also, we discovered during the course of the modeling that as the NO coverage increased, NO dissociation must slow down more than is predicted by the $\Theta^2_{*,\text{hollow}}$ and $\Theta^2_{*,\text{atop}}$ dependencies. In order to compensate for this effect we added the $\alpha_{NO}\Theta_{NO}$ term to the activation energy. This term increases the activation energy at high NO coverage and thus slows down the dissociation reaction. Since our TPD data are obtained over such a small temperature range, we have no way of knowing if this is the proper way to account for the NO inhibition of NO dissociation. For our purposes here, we only wanted to obtain the correct *rate* of NO dissociation and modification of the activation energy was a simple way to achieve this goal. It is most likely that the *proper* way to treat this self-inhibition of dissociation is through a higher than first-order dependence on $\Theta_{*,\text{atop}}$.

For N atom recombination we propose, based on our previous work, that N + N can react to form N_2, giving rise to at least three distinctly different N_2 desorption peaks depending on N coverage (30). This effect is discussed more fully in our previous paper (30) that examined N atom recombination in detail. However, for each of the three states the rate expression is:

$$R^{N_2}_{\text{form}} = \nu \exp\left(\frac{-(E_a - \alpha_N\Theta_N - \beta_O\Theta_O)}{RT}\right).$$

For O atom recombination we used, as previously proposed (12), O atom recombination rate expressions that have recombination occurring as a second-order process. This expression is valid for our experiment because O coverages are low enough so as not to populate the high-coverage, low-temperature first-order O_2 desorption state (12). For brevity we leave this rate expression out because, in the temperature range where N_2 and NO are desorbing, no measurable oxygen desorption occurs.

After we establish a rate expression for each step we must next choose a value for each of the rate parameters. Table 1 lists the values that were used to generate the model output shown in Figs. 7 and 8. Since one of our goals was to establish the rate constants for NO dissociation and NO desorption, these values were adjusted to obtain a good fit to the data. With regards to N atom recombination, we used the values determined in our previous paper (30) that examined the $N + N \rightarrow N_{2g}$ reaction as an isolated step. In that paper (30) we showed that if we treat N atom recombination as desorption from discrete TPD states, then three such states are required to accurately describe the observed TPD spectrum. The parameters for those three states are listed in Table 1 with only two modifications to those used previously (30). These modifications are to the β_O terms. The changes are relatively small and the differences between the two cases probably arise from different tendencies of N and O to form islands under the two different conditions of the study. We do not consider these small differences in the repulsive N–O interaction terms to be particularly important for the purpose of this paper.

As for the surface species conservation equations, they are:

$$-\frac{d\Theta_{NO}}{dt} = R^{NO}_{\text{desorp}} + R^{NO}_{\text{diss}}$$

$$-\frac{d\Theta_N}{dt} = 2 \times R^{N_2}_{\text{form}} - R^{NO}_{\text{diss}}$$

$$-\frac{d\Theta_O}{dt} = 2 \times R^{O_2}_{\text{form}} - R^{NO}_{\text{diss}}.$$

3. RESULTS AND DISCUSSION

3.1. NO TPD

Considering how closely linked our experiments are to previous papers on NO TPD from Rh surfaces (12, 25, 27–29), we felt that it was appropriate to include some NO TPD spectra in this paper. Figure 1 shows the N_2 that desorbs from a Rh(111) surface upon adsorption of different initial coverages of NO at 200 K. The complementary NO desorption, measured at the same time is shown in Fig. 2. The data were taken by using a linear temperature ramp of 10 K/sec. The QMS was multiplexed to monitor nine masses simultaneously. All of the NO exposures were done using a microchannel array doser. Because of the very high pumping speed of our chamber walls for NO, measured background pressures during the NO exposure were roughly 5×10^{-11} Torr above our base pressure of 7×10^{-11} Torr. However, the fact that we could saturate the entire surface with NO within about 15 sec suggests that the effective pressure 2–5 mm from the doser face was on the order of 10^{-7} Torr. Using this arrangement could prevent complications due to the slow pumping speed of NO in our system after extended high-pressure (10^{-8} Torr) exposures. However, we have no way to make reliable estimates of the actual exposures of NO in Fig. 1. When attempts were made to use background exposures to calibrate the doser we found that the measured background pressures were unreliable because of the high pumping speed of the chamber walls for NO. Because we could not calibrate our exposures in langmuirs, all exposures are given in doser-seconds and are only useful to give the relative exposures in two different experiments.

TABLE 1

Kinetic Parameters for the NO TPD Modeling

Reaction	Rate constant	Parameter	Value
$NO_a \rightarrow NO_g$	$\nu \exp\left(\frac{-E_a}{RT}\right)\Theta_{NO}$	E_a	29.7 kcal/mol
		ν	$4.6 \times 10^{14}\ s^{-1}$
$NO_a \rightarrow N_a + O_a$	$\nu \exp\left(\frac{-(E_a + \alpha_{NO}\Theta_{NO})}{RT}\right)$	E_a	17.5 kcal/mol
		α_{NO}	2.0
		ν	$2.1 \times 10^{10}\ s^{-1}$
$N_a + N_a \rightarrow N_{2g}$ State I	$\nu \exp\left(\frac{-(E_a - \alpha_N\Theta_N - \beta_O\Theta_O)}{RT}\right)$	E_a	35.7 kcal/mol
		α_N	10
		β_O	$13(\Theta_O \geq 0.2)$
			$2(\Theta_O \leq 0.2)$
		ν	$5.0 \times 10^{11}\ s^{-1}$
$N_a + N_a \rightarrow N_{2g}$ State II	$\nu \exp\left(\frac{-(E_a - \alpha_N\Theta_N - \beta_O\Theta_O)}{RT}\right)$	E_a	32.6 kcal/mol
		α_N	9
		β_O	3
		ν	$4.0 \times 10^{12}\ s^{-1}$
$N_a + N_a \rightarrow N_{2g}$ State III	$\nu \exp\left(\frac{-(E_a - \alpha_N\Theta_N - \beta_O\Theta_O)}{RT}\right)$	E_a	29.0 kcal/mol
		α_N	7.5
		β_O	5
		ν	$1.2 \times 10^{13}\ s^{-1}$

The data in Figs. 1 and 2 are in excellent agreement with previously published NO TPD data from Rh(111) (12). For very low NO coverages no NO desorbs from the surface but instead all of the NO dissociates, giving rise to a single N_2 desorption peak at 693 K that has been shown to be due to recombination desorption of N atoms (12, 13). Also in agreement with previous papers, we observe that the high-temperature edge of this desorption feature shifts markedly to lower temperature as the NO coverage is increased. This departure from pure second-order desorption kinetics arises due to the fact that surface oxygen from NO dissociation strongly accelerates the N + N reaction rate. This effect has been discussed fully in previous papers (12, 13, 30). As the NO coverage is increased, a second N_2 feature is observed at exactly the same time that NO desorption is first observed. This low-temperature, apparently first-order N_2 feature has been previously labeled δ-N_2 and was previously assigned to a NO + N $\rightarrow$ N_{2g} reaction (12, 15, 25). At the highest initial NO coverage, NO desorbs in a single peak at 433 K while δ-N_2 desorbs 15 K higher at 448 K, with the recombinative N_2 desorption feature occurring at 542 K.

3.2. $^{15}N + {}^{14}NO$: Assignment of the δ-N_2NO TPD Peak

In Fig. 3 we present the results of an experiment we designed to probe the origin of the δ-N_2 TPD peak. In this experiment we first prepared a surface with roughly 0.4 ML of ^{15}N atoms by the method outlined in Section 2.2. After initial adsorption of the ^{15}N atoms the surface was cooled to 200 K and a saturation exposure of ^{14}NO was then applied. During the resulting TPD experiment (Figs. 3 and 4) masses 14(^{14}N), 15(^{15}N), 28($^{14}N_2$), 29($^{14}N^{15}N$), 30($^{15}N_2$ and ^{14}NO), 31(^{15}NO), 44($^{14}N_2O$), 45($^{14}N^{15}NO$), and 46($^{15}N_2O$) were monitored. Figure 3 shows masses 30($^{15}N_2$ and ^{14}NO) and 31(^{15}NO) and makes one important point: no ^{15}NO was detected desorbing from the surface. The fact that no ^{15}NO is detected is strong evidence that no

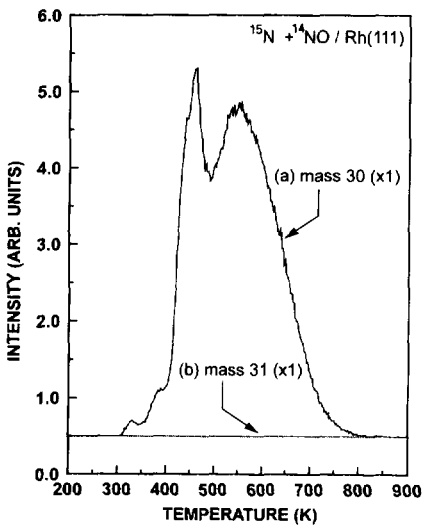

FIG. 3. Mass 30 (^{14}NO and $^{15}N_2$) and mass 31 (^{15}NO) desorption from a surface prepared with 0.4 ML of ^{15}N and saturation ^{14}NO added after ^{15}N adsorption.

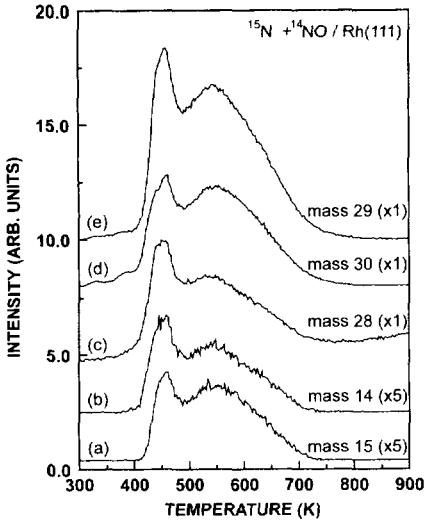

FIG. 4. Masses 14 (^{14}N), 15 (^{15}N), 28 ($^{14}N_2$), 29 ($^{14}N^{15}N$), and 30 (^{14}NO and $^{15}N_2$). Data are from the same surface as that for which the data in Fig. 3 were collected; 0.4 ML of ^{15}N and saturation ^{14}NO added after ^{15}N adsorption.

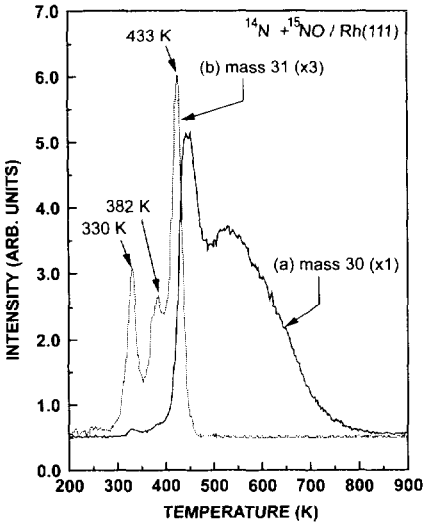

FIG. 5. Mass 30 ($^{15}N_2$) and mass 31 (^{15}NO) desorption from a surface prepared with 0.4 ML of ^{14}N and saturation ^{15}NO added after ^{14}N adsorption.

scrambling of the ^{15}N and ^{14}NO occurred during this experiment. Detection of ^{14}NO desorption (mass 30) is difficult since ^{14}NO is not separated from $^{15}N_2$ in this experiment. Figure 4 shows masses 14, 15, 28, 29, and 30. The general shape of the N_2 desorption peaks is the same as that of N_2 desorption in a typical NO TPD spectrum (Fig. 1). Because of this similarity we assume that the low-temperature δ-N_2 feature has the same origin in both our ^{15}N + ^{14}NO and NO TPD experiments. Looking first at masses 14 and 15 we see that there are very nearly the same amounts of ^{14}N and ^{15}N detected in the cracking pattern of the N_2 desorption feature. The important point is that for the coverages of ^{14}NO and ^{15}N chosen for this experiment roughly equal amounts of ^{14}N and ^{15}N are detected in the N_2 that desorbs from the surface. Looking next at masses 28, 29, and 30 (Fig. 4), one sees that the δ-N_2 peaks for these three masses are present in a 1 : 1.8 : 1 ratio for masses 28 : 29 : 30, respectively. The small amount of NO desorption (mass 30) overlapping with the leading edge of the δ-$^{15}N_2$ peak does not significantly affect this result because NO intensities in our QMS are roughly 10× weaker than N_2 signals (compare Figs. 1 and 2, noting that the y-axis scales are different). Using Figs. 1, 2, and 5 as a guide, we conclude that at the peak maximum of the δ-$^{15}N_2$ peak, the NO would contribute less than 5% of the total signal. At 433 K, the maximum for the NO desorption NO would constitute 45% of the leading edge of the δ-$^{15}N_2$ desorption peak. These relatively small overlaps in no way change the conclusions that can be drawn from these data; however, for completeness we performed the same experiment using ^{15}NO (31 amu), which does not overlap with any of the N_2 desorption peaks (see Figs. 5 and 6).

The fact that all three N_2 isotopic mixtures are observed in the desorption data of Fig. 4 proves that the δ-N_2 feature in NO TPD is due to N atom recombination and not a ^{15}N + ^{14}NO reaction. There are three possible outcomes from the isotope experiment that gave the data of Figs. 3 and 4. One possibility is that ^{14}NO could react cleanly with ^{15}N as an elementary step to produce $^{14}N^{15}N$. In this case only mass 29 would be detected in the δ-N_2 peak. This is clearly not the result that we observed and is the basis by which we rule out the NO + N reaction as the assignment

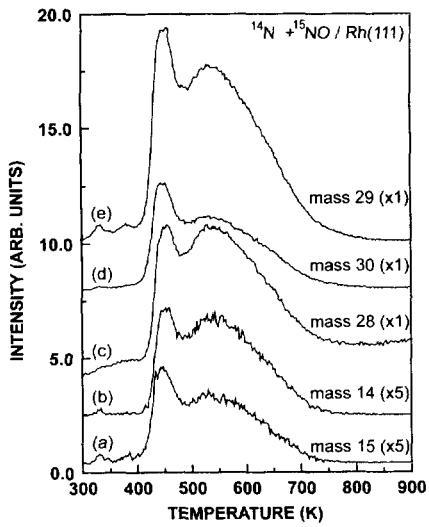

FIG. 6. Masses 14 (^{14}N), 15 (^{15}N), 28 ($^{14}N_2$), 29 ($^{14}N^{15}N$), and 30 ($^{15}N_2$) from the same surface as that for which the data in Fig. 5 were collected; 0.4 ML of ^{14}N and saturation ^{15}NO added after ^{14}N adsorption.

for the δ-N_2 feature. A second possibility is that the preadsorbed ^{15}N could scramble with the postadsorbed ^{14}NO, which would make the entire experiment inconclusive. However, this can be ruled out because no ^{15}NO desorbs from the surface (Fig. 3). The third possibility is that the postadsorbed ^{14}NO could dissociate to give ^{14}N atoms, which then react with the preadsorbed ^{15}N. Ideally, if ^{14}N and ^{15}N are present in a perfectly mixed pool with exactly the same concentrations, then masses 28, 29, and 30 would desorb in a 1:2:1 ratio, which is close to that which we measure (1:1.8:1). Based on the evidence of Figs. 2 and 3, we conclude that the δ-N_2 feature is due to recombinative desorption of N atoms.

For completeness we conducted the NO + N experiment in the reverse order by using ^{14}N and ^{15}NO. The results from these experiments are in complete agreement with the results shown in Figs. 3 and 4. The additional information gained from this experiment (Figs. 5 and 6) is that one can look at the ^{15}NO that desorbs from the surface at mass 31. Figure 6 shows exactly the same behavior as was observed in Fig. 4. In Fig. 5 we see that NO desorbs in three peaks at 330, 382, and 433 K. Beginning at the lowest temperature, this peak (330 K) is actually due to cracking of N_2O that desorbs from the surface prior to NO desorption. This conclusion is confirmed (Fig. 9) when one looks at the N_2O parent peak. We discuss N_2O formation below. The peak at 382 K is due to NO that desorbs in the presence of small amounts of surface oxygen. Previous papers (12) showed that adsorbed O shifts the NO desorption peak down in temperature from that observed from the clean surface. In our experiment the surface oxygen concentration is less than 0.1 ML and is the result of incomplete removal of O during N atom preparation. The largest peak in the mass 31 TPD spectrum is from NO that desorbs from the Rh(111) in the same manner as for a surface with only NO adsorbed (Fig. 2) (12). These results suggest that preadsorption of N does not strongly affect the surface binding energy of adsorbed NO. Further, comparison of the peak areas for both NO (Figs. 2 and 3) and N_2 (Figs. 1 and 4) shows that preadsorption of N atoms has very little effect on the saturation amount of NO that can be postadsorbed on the Rh(111) surface. We very roughly estimate that adsorption of 0.5 ML of N reduces the amount of NO that the Rh(111) surface can hold by about 20%. The implication of these results for Rh(111) surfaces are that (i) rate constants for NO desorption need not account for the effect of N on the NO desorption rate (reverse of step [2]), and (ii) NO and N are not in competition for the same sites and thus reaction mechanisms should not include terms by which adsorption of N atoms precludes the adsorption of NO.

3.3. *Modeling of NO TPD*

If the δ-N_2 feature is due to N atom recombination, why does this peak show apparent first-order behavior and the strong correlation of NO and δ-N_2 desorption? In order to answer this question and to learn more about NO dissociation rates at high coverages, we did some kinetic modeling of our NO TPD data. The details of our modeling are included in Section 2.3. The output of that model is shown in Figs. 7 and 8. Figure 7 shows the simulated NO TPD spectrum and Fig. 8 shows the simulated N_2 spectrum. Both

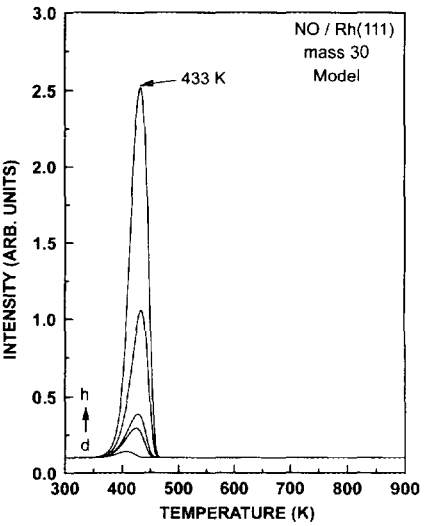

FIG. 7. Output of our kinetic model of NO desorption from a surface with adsorbed NO. NO coverages were selected to correspond with the companion data in Fig. 2. We assumed that saturation NO was 0.75 ML. Thus, the initial NO coverages were 0.22, 0.33, 0.36, 0.50, and 0.75 ML for curves (d)–(h), respectively.

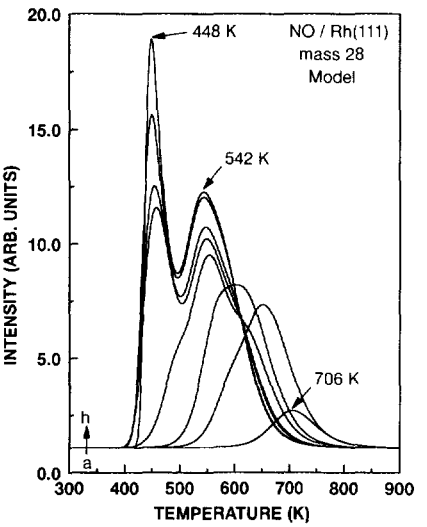

FIG. 8. Output of our kinetic model of N_2 desorption from a surface with adsorbed NO. Initial NO coverages were selected to correspond with the companion data in Fig. 1. We assumed that saturation NO was 0.75 MO. Thus, the initial NO coverages were 0.03, 0.14, 0.17, 0.22, 0.33, 0.36, 0.50, and 0.75 ML for curves (a)–(h), respectively.

these figures show peak widths and peak temperatures very similar to the experimental TPD data in Figs. 1 and 2; this shows that our simple model is a plausible explanation of the experimental data.

Two important points can be made based on our modeling. First, and most importantly, the model is able to accurately predict the apparent first-order δ-N_2 desorption kinetics as well as the 15 K temperature separation between the NO and δ-N_2 TPD peaks. Based on this modeling and our isotope experiments in Figs. 4–7, we conclude that the δ-N_2 is due to a N atom recombination reaction. The unusual kinetics observed in Figs. 1 and 2 are the result of the fact that the N + N reaction can be *faster than NO desorption or dissociation* if the N coverage is sufficiently high (30). This fact was previously reported by us in the first clean examination of the N + N reaction in the absence of competing reactions (30). A second crucial factor that leads to the apparent first-order N atom recombination kinetics is the experimentally observed fact that adsorbed NO strongly inhibits its own dissociation. At low NO coverages all of the NO dissociates below 325 K (13), well below the NO desorption (433 K) or δ-N_2 desorption (448 K) temperatures. But at sufficiently high NO coverages, NO dissociation is slowed so that no NO dissociation (and thus no N atom generation) occurs until some NO desorption occurs (15). As a result, at high NO coverages, large amounts of N atoms are generated at temperatures above which they would have desorbed if those same N atoms had been present on the surface at those lower temperatures. It is this effect that causes the δ-N_2 desorption to occur at a slightly higher temperature than NO desorption, concurrent with NO desorption, and with apparently first-order kinetics. For cases in which NO dissociation does not limit N atom formation, similar coverages of N atoms will desorb in a smooth second-order fashion (30).

A second important point was gained from modeling the NO TPD experiment. We feel that this modeling gives us a much better estimate for the NO dissociation *rate* in the limit of high NO coverages. Unfortunately, our current modeling capabilities are not sufficient to allow us to obtain a satisfying physical description of the dissociation process. At present we have made several crude assumptions as to the form of the dissociation rate equation in order to simplify the modeling. However, these assumptions do not affect our ability to assess the overall NO dissociation rate, NO $\rightarrow$ N + O, which we find is about 500 times slower than that reported for NO dissociation in the low coverage limit (11). Quite simply, if we used the much faster NO dissociation rate reported for very low coverages (11), then our model predicts two phenomena that are not experimentally observed. First, all of the NO will dissociate and none of the NO will desorb for initial NO coverages up to about 99% of saturation. This behavior is not experimentally observed (see Figs. 1 and 2). Second, NO dissociation will start at roughly 200 K for any NO coverage that is less than 99% saturated. This behavior is not experimentally observed either (13). For us to accurately model our NO TPD, the minimum difference in NO dissociation rates at low and high coverages (removing the first-order NO dependence) was roughly a factor of 6. Larger differences could be tolerated, which would lead to faster dissociation rates at low NO coverages. However, we are suspicious that the extremely fast NO dissociation rates, previously reported for low NO coverages, may be affected by dissociation at surface defects. It is our suggestion that for the purposes of understanding NO reduction under moderate pressure conditions (1–100 Torr), NO dissociation rates more like those reported in Table 1 should be used.

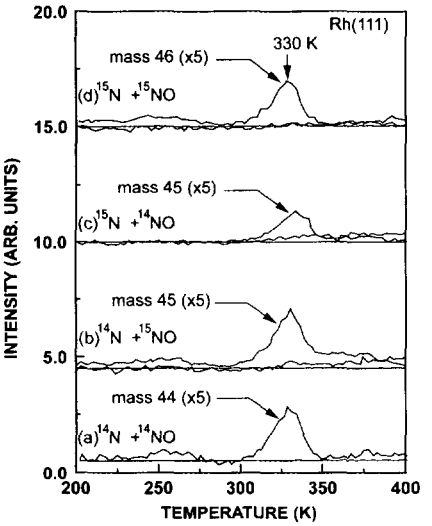

FIG. 9. Masses 44 ($^{14}N_2O$), 45 ($^{15}N^{14}NO$), and 46 ($^{15}N^{15}NO$) for four experiments that mixed different combinations of labeled N and NO. In all four experiments approximately 0.4 ML of N was preadsorbed on the surface and then saturation NO was postdosed on top of the N atom layer.

Finally, a third minor point came out of our modeling of NO TPD data: NO dissociation has a strong effect on the peak temperature and peak shape of the NO desorption feature. Basically, we were unable to reproduce the leading edge of the NO desorption feature using previously reported literature values (12). We suggest that a slightly higher E_a and preexponential factor give better fits to the actual experimental NO TPD data. It should be noted that the overall rate at the NO peak maximum is quite similar to that previously reported.

3.4. N_2O Formation from a NO + N Reaction

In contrast to the NO TPD experiment discussed above, when NO and N were reacted on Rh(111) we observed a small amount of N_2O formation under a very limited set of experimental conditions. Figure 9 shows the results of four experiments in which different combinations of la-

beled NO and N were reacted. In each case approximately 0.4 ML of N atoms were adsorbed and then saturation NO was added to that surface. For each experiment three masses (44, 45, and 46) are shown. In Fig. 9 we focus on only the low-temperature region where N_2O formation is observed. In all of the experiments two results are consistently observed. First, the N_2O formed had the expected mass, and only that for a clean NO + N reaction. For instance, for the top set of spectra in Fig. 9c, ^{15}N was reacted with ^{14}NO, which produced only mass 45. Second, from the cracking pattern of N_2O we can tell that the N–O bond remains intact during N_2O formation. Our evidence for this conclusion is that the NO in the cracking pattern is always labeled by the same isotope as that of the initially adsorbed NO. Thus for the experiment shown in Fig. 9c in the cracking pattern for the N_2O we detected $^{15}N^{14}N$ and ^{14}NO. These two results prove that the N_2O we observed in this experiment was the result of a NO + N reaction and not a three-body N + N + O reaction or a NO + NO reaction. By way of caution we should point out that the amount of N_2O formed in this experiment was extremely small. We very roughly estimate that about <0.1 ML of NO reacts to form N_2O in the experiments shown in Fig. 9. Further, we observed that three conditions must be met before N_2O could be formed via the pathway in Fig. 9. They are: (i) the surface must be saturated with NO, including a small compression state at the leading edge of the NO desorption peak; (ii) initial N coverages must be higher than 0.25 ML; and (iii) contaminant concentrations (either O or CO) must be less than 0.1 ML. Further, we noted that N_2O formation ceased when the compressed NO desorbed from the surface. The fact that N_2O formation is very sensitive to surface coverages explains why previous experiments by Fisher and co-workers were unsuccessful in producing N_2O. Apparently, their N atom coverages, formed by thermal methods, were too low to allow for N_2O formation. Given the remarkable sensitivity of this N_2O formation pathway to surface coverages of all species (but especially to NO) we feel that it is unlikely that this is the pathway by which N_2O is formed under high-pressure conditions. We say this primarily because, at high pressures, N_2O formation over Rh(111) is marked by its incredible insensitivity to reaction conditions (22). It is our suspicion that a second, slower pathway to N_2O formation exists which is responsible for the N_2O formation observed over Rh(111) under moderate-pressure conditions. We assume that the reason that we do not observe this N_2O formation route in our experiments is that it is slower than NO desorption and therefore would occur at temperatures above which NO desorbs.

3.5. Implications for the NO–CO Reaction at Higher Pressures

Based on the results of the experiments reported here, we feel that we have a better understanding of the rates of some of the elementary steps in the NO–CO mechanism. At present we have not tried to apply these rate constants in a detailed kinetic mechanism that attempts to model the NO–CO reaction rates at moderately high pressures. However, we feel that we can make some recommendations as to how to use the information we have gained to understand that reaction mechanism. First, and most importantly, our NO + N isotope experiments conclusively show that the δ-N_2 NO TPD peak is not due to an NO + N reaction. Assignment of this N_2 feature as a NO + N reaction was the primary piece of experimental evidence that led to the inclusion of the NO + N $\rightarrow$ N_{2g} reaction in the NO–CO mechanism. Although our data do not prove that this reaction does not occur, they do show that there is no experimental evidence for this reaction. Based on this observation, we suggest that NO + N $\rightarrow$ N_{2g} be included in the mechanism *only if required* to explain the observed reaction kinetics and not as an experimentally confirmed reaction step. Second, our reexamination of the NO TPD experiment, coupled with more detailed modeling, has given us greater insight into the rates for NO dissociation and NO desorption. Our modeling results suggest that NO dissociation at high NO coverage is roughly 500× slower than for the low coverage limit. We suggest that a rate constant more like that in Table 1 is applicable for NO coverages above 0.1 ML. We caution that the exact form of the rate expression is in doubt at this time and thus the values given in Table 1 may not extrapolate well to higher temperatures. However, in the 400 K regime at $\Theta_{NO} \geq 0.1$ ML, we are confident that NO dissociation is significantly slower than previously thought. Third, our modeling also suggests that slightly different NO desorption rate parameters are more accurate than those previously reported. Our modeling suggests that a higher preexponential factor is required to accurately predict the leading edge characteristics of the NO desorption feature. Previously reported rate constants used the peak width and peak temperature to extract the NO desorption rate parameters. Our results suggest that this leads to small errors because NO dissociation significantly affects the surface NO coverages and thus NO desorption rates on the high-temperature side of the peak maximum.

4. CONCLUSIONS

We have studied the reaction of isotopically labeled NO and N mixtures on Rh(111) and have reexamined and modeled the NO TPD experiment. Our results show that the δ-N_2 feature, commonly associated with an NO + N reaction, is in fact due to N atom recombination that is rate-limited by NO dissociation. In addition, we offer new estimates for the rate of NO dissociation at NO coverages above 0.1 ML and for the rate of NO desorption. These results are important for obtaining a better understanding

of the mechanism by which NO is reduced by CO over Rh catalysts.

ACKNOWLEDGMENTS

K. Y. S. Ng acknowledges partial financial support from General Motors R&D for his sabbatical leave to perform this research.

REFERENCES

1. Hecker, W. C., and Bell, A. T., *J. Catal.* **84,** 200 (1983).
2. Hecker, W. C., and Bell, A. T., *J. Catal.* **85,** 389 (1984).
3. Cho, B. K., Shanks, B. H., and Bailey, J. E., *J. Catal.* **115,** 486 (1989).
4. McCabe, R. W., and Wong, C., *J. Catal.* **121,** 422 (1990).
5. Cho, B. K., *J. Catal.* **131,** 74 (1991).
6. Oh, S. H., *J. Catal.* **124,** 477 (1990).
7. Cho, B. K., *J. Catal.* **138,** 255 (1992).
8. Leclercq, G., Dathy, C., Mabilon, G., and Leclercq, L., *Stud. Surf. Sci. Catal.* **71,** 181 (1991).
9. van den Bosch-Driebergen, A. G., Kieboom, M. N. H., van Dreumel, A., Wolf, R. M., van Delft, F. C. M. J. M., and Nieuwenhuys, B. E., *Catal. Lett.* **2,** 273 (1989); **2,** 235 (1989).
10. Oh, S. H., and Carpenter, J. E., *J. Catal.* **98,** 178 (1986).
11. Oh, S. H., Fisher, G. B., Carpenter, J. E., and Goodman, D. W., *J. Catal.* **100,** 360 (1986).
12. Root, T. W., Schmidt, L. D., and Fisher, G. B., *Surf. Sci.* **134,** 30 (1983); **150,** 173 (1985).
13. Root, T. W., Fisher, G. B., and Schmidt, L. D., *J. Chem. Phys.* **85,** 4679 (1986).
14. Root, T. W., Fisher, G. B., and Schmidt, L. D., *J. Chem. Phys.* **85,** 4687 (1986).
15. Schwartz, S. B., Fisher, G. B., and Schmidt, L. D., *J. Phys. Chem.* **92,** 389 (1988).
16. Peden, C. H. F., Goodman, D. W., Blair, D. S., Fisher, G. B., Berlowitz, P. J., and Oh, S. H., *J. Phys. Chem.* **92,** 1563 (1988).
17. Hendershot, R. E., and Hansen, R. S., *J. Catal.* **98,** 150 (1986).
18. Wolf, R. M., Bakker, J. W., and Nieuwenhuys, B. E., *Surf. Sci.* **246,** 135 (1991).
19. Wolf, R. M., Siera, J., van Delft, F. C. M. J. M., and Nieuwenhuys, B. E., *Faraday Discuss. Chem. Soc.* **87,** 1989 (275).
20. Siera, J., Rutten, F., and Nieuwenhuys, B. E., *Catal. Today* **10,** 353 (1991).
21. Hirano, H., Yamada, T., Tanaka, K. I., Siera, J., Cobden, P., and Nieuwenhuys, B. E., *Surf. Sci.* **262,** 97 (1992).
22. Belton, D. N., and Schmieg, S. J., *J. Catal.* **144,** 9 (1993).
23. Peden, C. H. F., Belton, D. N., and Schmieg, S. J., submitted for publication.
24. Chan, C.-M., Aris, R., and Weinberg, W. H., *Appl. Surf. Sci.* **1,** 360 (1978).
25. Chin, A., and Bell, A. T., *J. Phys. Chem.* **87,** 3700 (1983).
26. Campbell, C. T., and White, J. M., *Appl. Surf. Sci.* **1,** 347 (1978).
27. Zafiris, G. S., and Gorte, R. J., *J. Catal.* **132,** 275 (1991).
28. Ho, P., and White, J. M., *Surf. Sci.* **137,** 103 (1984).
29. Baird, R. J., Ku, R. C., and Wynblatt, P., *Surf. Sci.* **97,** 346 (1980).
30. Belton, D. N., DiMaggio, C. L., and Ng, K. Y. S., *J. Catal.* **144,** 273 (1993).